Global non-hydrostatic modelling using Voronoi meshes: The MPAS model

William C. Skamarock, Joseph B. Klemp, Michael Duda, Laura Fowler and Sang-Hun Park

National Center for Atmospheric Research
Boulder, Colorado, USA, 80307-3000
skamaroc@ucar.edu

ABSTRACT

We outline the formulation of a fully compressible nonhydrostatic model discretized on centroidal Voronoi meshes using a C-grid staggering of the prognostic variables. The Voronoi meshes are unstructured meshes that permit variable horizontal resolution, and our nonhydrostatic model solves the equations of motion directly on these unstructured meshes. The unstructured variable-resolution meshes allow for applications beyond uniform-resolution global NWP and climate prediction, in particular allowing embedded high-resolution regions for regional NWP and regional climate applications. The rationale for aspects of this formulation are discussed, and results from tests for large-scale flow on the sphere and for nonhydrostatic flows on Cartesian planes are presented.

1 Introduction

Global atmospheric models have typically used latitude-longitude grids for their discretization. The use of these meshes necessitates the use of polar filters and other extensions to the base numerical schemes due to the convergence of grid lines at the poles. Spherical transform methods, while not requiring polar filtering, do not scale optimally with increasing resolution, and the semi-Lagrangian transport with which they are often paired needs special attention in the polar regions. Finite difference and finite-volume methods on latitude-longitude meshes, and spherical transform methods, do not scale (map) well onto the latest generations of supercomputers that rely on large numbers of distributed-memory processing elements.

We are constructing a global fully compressible nonhydrostatic model using finite-volume numerics discretized on centroidal Voronoi (nominally hexagonal) meshes using C-grid staggering of the prognostic variables based on the work of Thuburn et al. (2009) and Ringler et al. (2010). This model is called the Model for Prediction Across Scales (MPAS), and it is a collaborative project being led by the National Center for Atmospheric Research (NCAR) and Los Alamos National Lab (LANL). NCAR is responsible for developing the MPAS atmospheric component, LANL is responsible for the ocean component, with joint development of the shared software infrastructure. The centroidal Voronoi meshes allow for local refinement, and the horizontal mesh is unstructured. In the following sections we present the equations and the finite-volume split-explicit discretization used in the unstructured mesh solver, we discuss some aspects of the variable unstructured mesh and the considerations involving the discretizations, and we present results from test simulations at large scales on the sphere and at convective scales on Cartesian planes. The test simulations indicate that the solver is performing as well or better than existing icosahedral mesh models based on the results presented here, and on shallow water tests and theoretical considerations presented in the previous work of Ringler et al. (2010).

2 Governing Equations and Discretization

2.1 Continuous equations

We cast the governing equations in terms of a hybrid height-based vertical coordinate ζ following Klemp (2011). In this formulation the height of the coordinate surface

$$z = \zeta + A(\zeta)\, h_s(x,y,\zeta), \tag{1}$$

where z_t is the constant height of the upper boundary, ζ represents the nominal heights (ignoring terrain) of the coordinate surfaces and $A(\zeta)$ defines the relative weighting between the terrain-following coordinate and the pure height coordinate, such that $0 \le A \le 1 - \zeta/z_t$. For $A(\zeta) = 1 - \zeta/z_t$ and $h_s(x,y,\zeta) = h(x,y)$ (the terrain height) we recover the traditional terrain-following height coordinate and for $A(\zeta) = 0$ we recover a pure height coordinate. The array h_s can be specified to produce increased smoothing of the terrain influence with height with the requirement that $h_s(x,y,0) = h(x,y)$. As described in Klemp (2011), we can choose $A(\zeta)$ and h_s to control the amount and scale of terrain influence on the vertical coordinate.

We define the flux variables

$$(U,V,\Omega,\Theta,Q_j) = \tilde{\rho}_d \cdot (u,v,\dot{\eta},\theta,q_j) \tag{2}$$

to provide mass and scalar conservation, where ρ_d is the density of dry air, $\tilde{\rho}_d = \rho_d/\zeta_z$, and q_j represents the mixing ratio of the respective water species. The inviscid prognostic nonhydrostatic equations are written in flux form using these variables, with the horizontal momentum equations expressed in vector-invariant form to help achieve desired conservation properties:

$$\begin{aligned}
\frac{\partial \boldsymbol{V}_H}{\partial t} =& -\frac{\rho_d}{\rho_m}\left[\boldsymbol{\nabla}_\zeta\left(\frac{p}{\zeta_z}\right) - \frac{\partial \boldsymbol{z}_H p}{\partial \zeta}\right] - \eta\, \boldsymbol{k}\times\boldsymbol{V}_H \\
& - \boldsymbol{v}_H \boldsymbol{\nabla}_\zeta \cdot \boldsymbol{V} - \frac{\partial \Omega \boldsymbol{v}_H}{\partial \zeta} - \rho_d \boldsymbol{\nabla}_\zeta K - eW\cos\alpha_r - \frac{uW}{r_e} + \boldsymbol{F}_{V_H}, \qquad (3)\\
\frac{\partial W}{\partial t} =& -\frac{\rho_d}{\rho_m}\left[\frac{\partial p}{\partial \zeta} + g\tilde{\rho}_m\right] - \left(\boldsymbol{\nabla}\cdot\boldsymbol{v}W\right)_\zeta \\
& + \frac{uU+vV}{r_e} + e\,(U\cos\alpha_r - V\sin\alpha_r) + F_W, \qquad (4)\\
\frac{\partial \Theta_m}{\partial t} =& -\left(\boldsymbol{\nabla}\cdot\boldsymbol{V}\,\theta_m\right)_\zeta + F_{\Theta_m}, \qquad (5)\\
\frac{\partial \tilde{\rho}_d}{\partial t} =& -\left(\boldsymbol{\nabla}\cdot\boldsymbol{V}\right)_\zeta, \qquad (6)\\
\frac{\partial Q_j}{\partial t} =& -\left(\boldsymbol{\nabla}\cdot\boldsymbol{V}\,q_j\right)_\zeta + \rho_d S_j + F_{Q_j}, \qquad (7)
\end{aligned}$$

and pressure is obtained diagnostically from the equation of state:

$$p = p_0\left(\frac{R_d\zeta_z\Theta_m}{p_0}\right)^\gamma, \tag{8}$$

with $\gamma = c_p/c_v$. Here, $\boldsymbol{V} = (U,V,\Omega)$, ρ_m is the density of moist air,

$$\frac{\rho_m}{\rho_d} = 1 + q_v + q_c + q_r + \ldots, \tag{9}$$

and θ_m is a modified moist potential temperature,

$$\theta_m = \theta[1 + (R_v/R_d)q_v]. \tag{10}$$

In (3), $\eta = \boldsymbol{k} \cdot \boldsymbol{\nabla} \times \boldsymbol{v}_H + f$ is the absolute vertical vorticity, and $K = |\boldsymbol{v}_H|^2/2$ is the horizontal kinetic energy. The metric terms associated with the vertical coordinate transformation are represented by $\boldsymbol{\nabla}\zeta = (\zeta_x, \zeta_y, \zeta_z)$, with $\boldsymbol{\zeta}_H = (\zeta_x, \zeta_y)$ and $\boldsymbol{z}_H = -\boldsymbol{\zeta}_H/\zeta_z$. $\Omega = \boldsymbol{V} \cdot \boldsymbol{\nabla}\zeta$ is the component of the mass flux normal to the coordinates surfaces in the transformed coordinate. In the curvature and Coriolis terms in (3) and (4), $f = 2\Omega_e \sin\psi$, $e = 2\Omega_e \cos\psi$, ψ is the latitude, Ω_e is the angular rotation rate of the earth, r_e is the earth radius, and α_r is the rotation angle between the line normal to the horizontal velocity and the meridians.

2.2 Discretization

In the MPAS model, the continuous equations are spatially discretized on a unstructured C-grid centroidal Voronoi mesh following Thuburn et al. (2009) and Ringler et al. (2010). Nominally uniform traditional icosahedral meshes as well as variable resolution meshes can be generated for the sphere, for regional domains on the sphere, and for Cartesian planes using techniques described in Ringler et al. (2008).

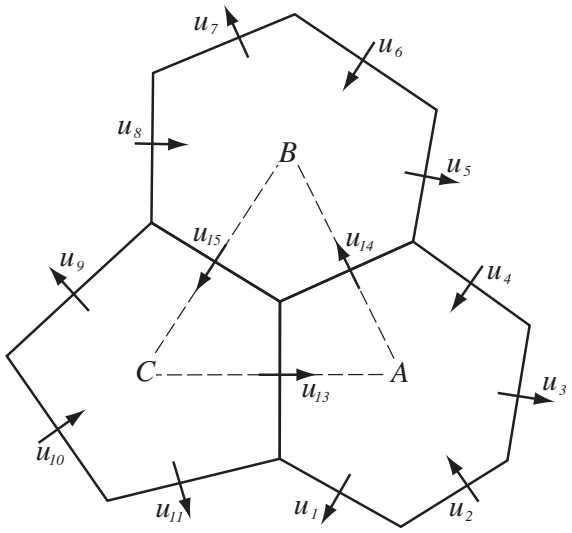

Figure 1: The Voronoi mesh

A horizontal C-grid Voronoi mesh is depicted in figure 1. The horizontal momentum normal to the cell edge is prognosed at the cell edges and the coupled potential temperature Θ_m, density $\tilde{\rho}$ and moisture Q_j are prognosed at the cell centers where they represent cell-averaged values in the finite volume formulation. The vertical momentum is prognosed on the vertical cell face located half a grid level above and below the cell center, consistent with a 3D C-grid discretization. All other quantities are diagnosed from the prognostic variables, e.g. pressure (8). The tangential component of the horizontal momentum, appearing in the horizontal momentum equation (3), is diagnosed following Thuburn et al. (2009), and the absolute vertical vorticity η and kinetic energy K in (3) are diagnosed following Ringler et al. (2010). These horizontal discretization techniques for the C grid do not suffer from the problems of the non-stationary geostrophic mode. The horizontal discretization exactly conserves mass (to machine roundoff), and, in the 2D shallow water framework, exactly conserves potential vorticity and conserves energy to the time truncation error (Ringler et al., 2010)

The fully compressible nonhydrostatic equations (3) – (7) are solved using the time-split integration technique described in Klemp et al. (2007) for height-coordinate equations. We use the third-order Runge-Kutta scheme of Wicker and Skamarock (2002) with the time-split algorithm. The use of the vector-invariant form of the horizontal momentum equation (3) does not complicate the solution proce-

dure, but note that we cast this equation in flux form to facilitate the acoustic solve. This gives rise to the additional term $\boldsymbol{v}_H \boldsymbol{\nabla}_\zeta \cdot \boldsymbol{V}$ that does not appear in non-flux-form equations that are usually used in this context, e.g. Ringler et al. (2010).

The transport scheme used for the flux divergence calculations in (5) and (7) on the irregular Voronoi ($\sim$hexagonal) mesh is described in Skamarock and Gassman (2011). It uses nominally third and fourth order approximations for projecting the scalar value to the cell edge in the conservative flux-divergence calculation. The mass flux divergence in (6) is approximated by averaging the cell averaged values of $\tilde{\rho}$ to the cell face from the two cells sharing the face (see Thuburn et al., 2009). We use the mass flux that is time-averaged over the acoustic steps for scalar transport, thus maintaining consistency between the scalar transport and the continuity equation. As explained in Klemp et al. (2003), it is important to maintain consistency between the transport operator and the metric terms associated with the terrain transformation. In MPAS this requires that the diagnosis of the transformed vertical velocity Ω be consistent with the advection operator used in the thermodynamic equation (5). To satisfy this requirement, we formulate the transformed vertical velocity for cell i as

$$\begin{aligned} \Omega_i &= \boldsymbol{V} \cdot \boldsymbol{\nabla} \zeta = \zeta_z \boldsymbol{V} \cdot \boldsymbol{\nabla} (z - z_i) \\ &= \zeta_z \left[\boldsymbol{\nabla} \cdot \boldsymbol{V} (z - z_i) - (z - z_i) \boldsymbol{\nabla} \cdot \boldsymbol{V} \right] \\ &= \zeta_z \boldsymbol{\nabla} \cdot \boldsymbol{V} (z - z_i), \end{aligned} \tag{11}$$

where z_i is the coordinate-surface height at cell i for which Ω_i is being computed. We apply the Skamarock and Gassman (2011) scheme to the right-hand-side of (11) thus satisfying the consistency requirement. The expensive part of the Skamarock and Gassman scheme, evaluating $(z - z_i)$ at the cell faces, can be computed and the results stored before integration begins, thus there is little additional cost in implementing the Klemp et al. (2003) consistency requirement.

2.3 Nonuniform meshes

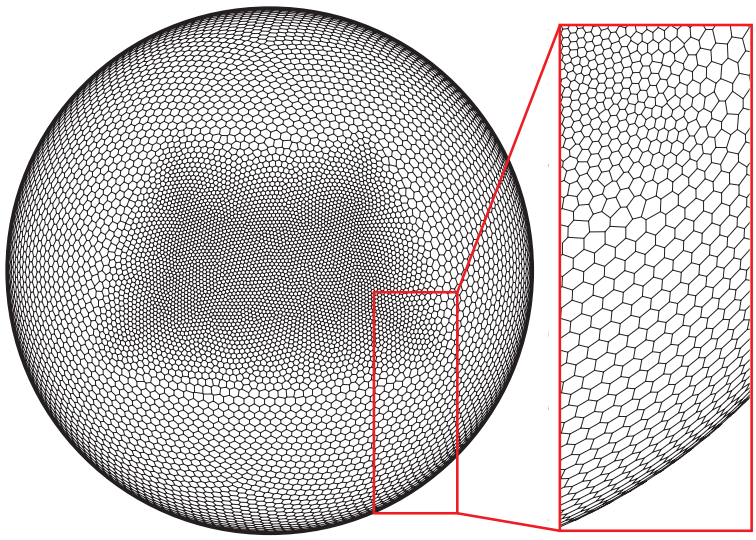

Figure 2: Variable resolution Voronoi mesh

For uniform resolution simulations on the sphere, the spherical centroidal Voronoi tesselation is the icosahedral mesh, and results for shallow water tests using this mesh are given in Ringler et al. (2010). Our intended applications also include regional NWP and regional climate, for which the Voronoi

meshes can be generated using a specified non-uniform mesh density. Figure 2 depicts a variable resolution mesh with refinement embedded. The global mesh is represents a single mesh and it is conforming - there are no hanging nodes in this mesh. The resolution resolution changes smoothly from the coarse to the fine mesh regions. We have significant flexibility in the mesh generation process, which requires only a user-specified density function (Ringler et al., 2008).

We expect that smooth mesh transitions will ameliorate many problems encountered in traditional approaches to mesh refinement such as the use of embedded nests where the change in resolution is abrupt, and in the grid stretching procedures used in some rectangular mesh models that can produce some regions of very anisotropic cells and that is usually limited to refinement in a single region. Initial tests of MPAS on the sphere and at convective scales on Cartesian doubly-periodic planes using the smooth mesh transitions are producing consistent results without noticeable distortion.

2.4 Discretization considerations

There are a number of new aspects in the MPAS solver formulation, compared with other icosahedral-mesh formulations, that appear to provide beneficial characteristics in the solver for global multiscale (hydrostatic- and nonhydrostatic-scale) atmospheric simulation.

The first significant advance in the MPAS formulation is the formulation for the C-grid staggering of the prognostic variables. Ničković et al. (2002) examined the problem of the hexagonal C-grid geostrophic mode. The problem arises because the tangential velocity needs to be reconstructed from the prognosed normal velocities on the cell faces in order to evaluate the Coriolis term, and Ničković et al showed that the stationary geostropic mode in the linearized shallow water equations will be nonstationary using the most obvious reconstruction of the tangential velocity. The nonstationary geostrophic mode renders the scheme useless for global applications. Thuburn (2008), Thuburn et al. (2009) and Ringler et al. (2010) developed a method to reconstruct the tangential velocity such that the geostrophic mode remains stationary and also that allows for potential vorticity conservation, enstrophy conservation or dissipation following Sadourny and Basdevant (1985), and energy conservation to the time truncation error. This critical advance is based on the constraint that the horizontal mass divergence on the triangular mesh (the dashed triangular cell in figure 1; the dual of our hexagonal mesh), that is computed using the reconstructed tangential velocities, be equal to the area-weighted sum of the divergences in the hexagons underlying the triangular cell. This formulation makes possible the conservation of potential vorticity, enstrophy and energy, and these conservation properties can be considered a generalization of the conservative rectangular mesh discretizations of Sadourny (1975) and Arakawa and Lamb (1981).

Our use of the C grid staggering is guided by theory and by practical experience. Mesoscale and cloud-scale motions are dominated by horizontally divergent motions, and C-grid staggering provides twice the resolution of divergent modes than the unstaggered (A) grid and it does not require any averaging of the velocities or pressures as is required on the A, B, D and E-grid staggerings. Pressure and velocity averaging lead to stationary grid-scale modes that must be filtered, and the parasitic modes associated with the divergence and pressure gradient terms will require a higher level of filtering on these meshes. Our experience is that the level of filtering needed on these other meshes is considerably higher than that needed to provide sinks for the downscale energy and enstrophy cascades in our full nonlinear simulations using the C-grid staggering. In practice, we find that solvers not using C-grid staggering need finer meshes to produce similarly resolved features (such as clouds). Our experience also indicates that higher-order differencing of the mass divergence and pressure gradient terms does not appreciably change these results; stationary modes remain, increased filtering is still needed on the non-C-grid meshes, and higher mesh densities are still needed to produce comparably-resolved solutions. Generally speaking, all meshes can be made to work with some level of filtering; the choices affect scheme efficiency (accuracy versus cost), and we have found that the C-grid discretization results in the highest efficiency.

The analysis of Randall (1994) examining geostrophic adjustment indicates that the C-grid staggering is not optimal for large-scale flows. Our intended applications for MPAS are cell spacings of order 100 km and less. Our tests to date show that MPAS produces solutions similar in accuracy to other finite-volume and finite difference models for large scale flows (based on results in Ringler et al. (2010) for shallow-water tests, and our results for the Jablonowski and Williamson (2006) baroclinic wave tests). We have not identified any problems arising from the C-grid discretization, neither with the computational Rossby modes addressed in Thuburn et al. (2009), nor with other potential inaccuracies noted in the literature.

The second advance incorporated into MPAS is the use of advection schemes making use of higher-order operators. Unstructured, irregular meshes often use simple nominally second order operators within the advection algorithms. For example, the flux divergence term in the scalar conservation equation requires that mass flux be evaluated at the cell edge, and a second-order formulation could use the average of the scalar values in the two cells sharing that edge. However, these simple schemes do not produce solutions on hexagonal meshes that are as accurate as our rectangular mesh cloud and mesoscale models. We have implemented a scheme for use with the MPAS Runge-Kutta time integration, based on the 3rd and 4th order transport schemes used in the ARW model Skamarock and Klemp (2008) using least-squares polynomial fits for scalars, that allow us to reproduce the accuracy we obtain on the regular rectangular meshes on the irregular MPAS meshes. Without the use of these more accurate schemes, we are not able to produce solutions with accuracy similar to ARW.

Finally, unstructured mesh solvers such as MPAS make use of indirect addressing when building the horizontal operators during a timestep. We keep vertical columns contiguous in memory in our Fortran implementations, and we find that the our solvers have similar computational efficiencies as our rectangular (structured) grid solvers. MacDonald et al. (2010) have examined the question of efficiency in 3D atmospheric solvers and find that, on cache-based computer architectures, having vertical columns contiguous in memory produces solvers as efficient as their structured-mesh counterparts.

3 Simulations on the sphere

A standard test for 3D solvers on the sphere is the Jablonowski and Williamson (2006) baroclinic wave test. We have simulated the test as described in the reference using horizontal mesh resolutions from approximately 480 km cell-center spacing (2562-cell icosahedral mesh) to approximately 30 km cell spacing (655362-cell icosahedral mesh). The initial state consists of identical zonally symmetric unstable jets in both the northern and southern hemispheres. The initial state represents an unstable steady-state solution, and a baroclinic wave is triggered with a small perturbation in the northern hemisphere zonal wind. Figure 3 depicts the surface pressure at day 9 for the 120 km average-cell-spacing mesh.

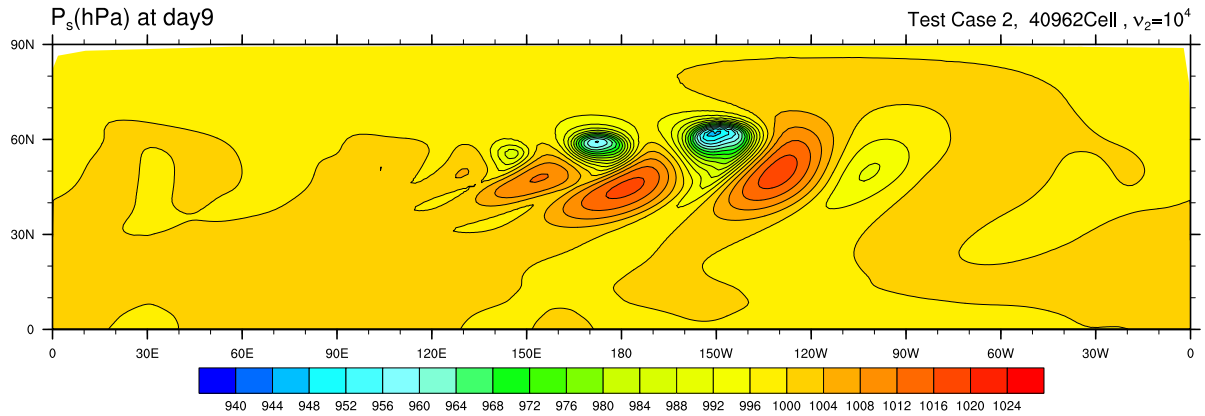

Figure 3: Jablonowski and Williamson baroclinic wave test simulation.

The solution on this mesh and for the other mesh densities compare well with the published solutions in Jablonowski and Williamson (2006). We have also used this test case to examine model behavior using different advection schemes. We have found that using higher-order schemes for the transport of potential temperature in this dry simulation significantly improves the accuracy of the solution with respect to both phase and amplitude errors (Skamarock and Gassman, 2011).

The baroclinic wave train depicted in figure 3 is initiated using an unbalanced perturbation. We have also computed the most unstable normal mode for the jet, and the structure of the normal mode in the surface pressure field is depicted in figure 4.

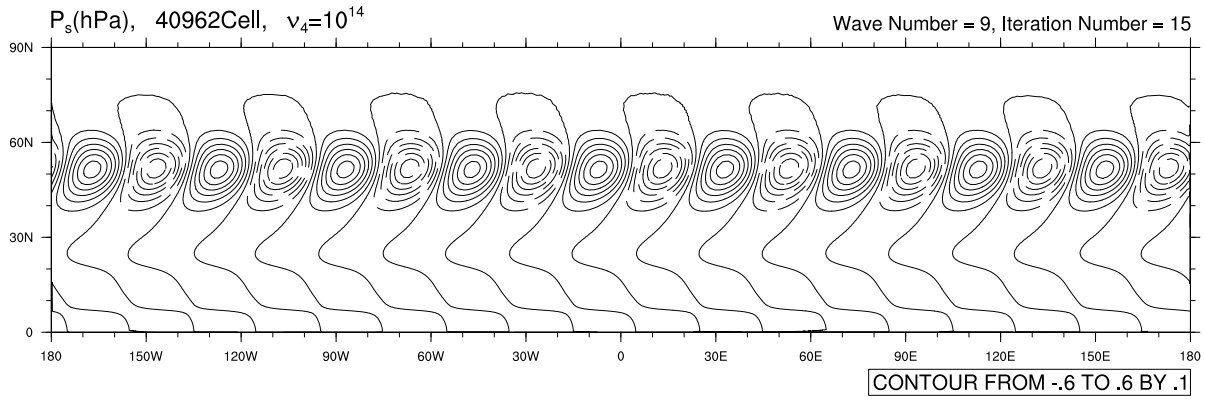

Figure 4: Surface pressure for the fastest growing normal mode of the Jablonowski and Williamson baroclinic jet.

The most unstable mode has wavenumber 9. The normal mode is computed by putting in a perturbation at a particular zonal wavenumber, integrating forward in time with periodic rescaling of the perturbation fields. Note that the icosahedral mesh used in these simulations inserts its own perturbation into the solution in the form of a zonally varying truncation error in wavenumber multiples of 5, and the normal mode depicted in these results shows good wavenumber 9 symmetry even though the icosahedral grid does not promote this wavenumber mode.

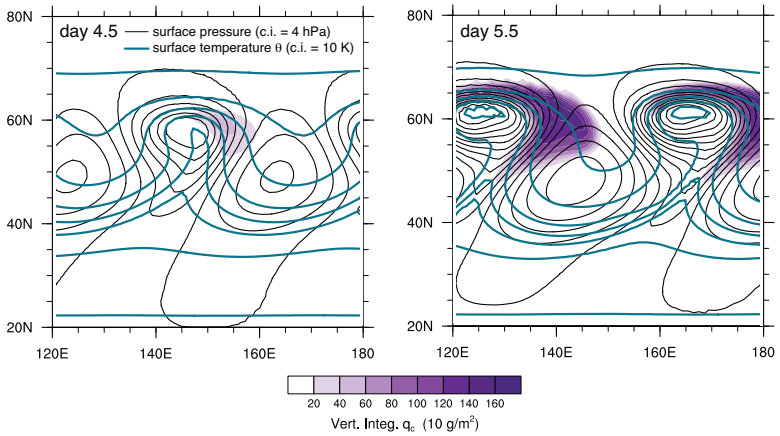

Figure 5: Moist baroclinic wave simulation.

We have used the normal mode initialization and added moisture to the initial state along with Kessler warm-rain microphysics to test the model response at large scales to stable precipitation processes. The initial moisture distribution specifiies an atmosphere with approximately 40% relative humidity below approximately 500 hPa decreasing to zero quickly above that level. The moist baroclinic wave simulation at days 4.5 and 5.5 (beginning from the amplitude depicted in figure 4) is shown in figure

5. The solutions remain smooth and well resolved, and the addition of latent heating has not resulted in any decrease in solver robustness at these scales. We are in the process of implementing a complete set of physics for full NWP simulations, and preliminary tests indicate that the solver retains its robustness for the case of unstable convection and parameterized convection in similar baroclinic wave simulations but with increased moisture.

4 Convective-scale simulations

It is very difficult to test the nonhydrostatic response of global solvers because very high resolutions are needed to resolve nonhydrostatic scales, particularly convection where cell spacings of a few kilometers or less are needed. An advantage of the unstructured Voronoi mesh and solver is that we can use our solver on both the sphere and on doubly-periodic Cartesian planes. We have performed extensive tests of the solver for nonhydrostatic scale motions in the Cartesian planes using both 2D (x,z) and 3D test cases, including mountain waves, 2D and 3D squall lines and 3D supercells thunderstorms. For the mountain wave cases we have exact linear and nonlinear solutions, and these tests have helped us verify the correctness of our coding.

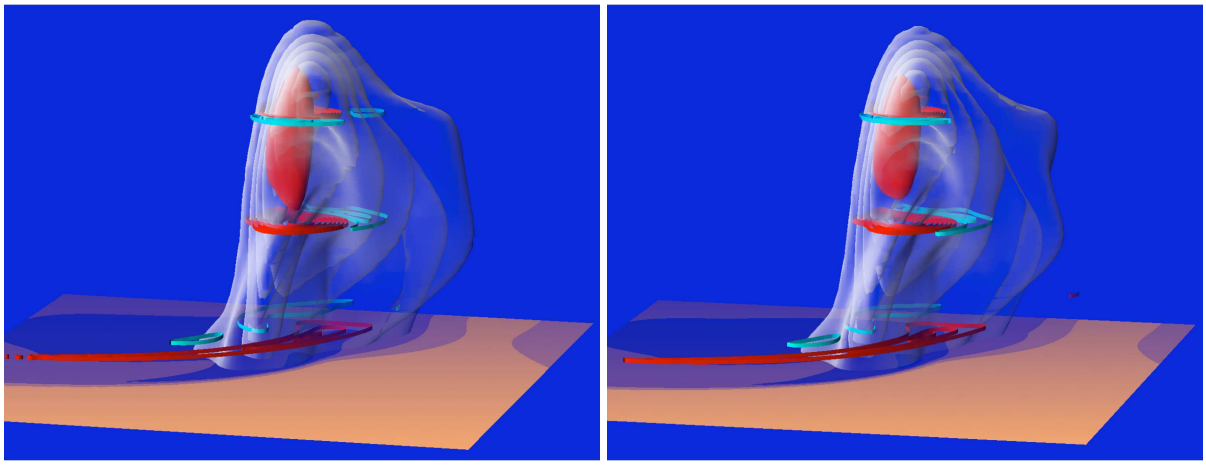

(a) Hexagonal mesh simulation (b) Rectangular mesh simulation

Figure 6: 3D depiction of supercell simulation results at 6000 seconds. approximately 500 m cell spacing horizontally and 500 m vertical spacing. The vertical velocity is contoured at 1, 5, and 10 km (c.i. = 3 m/s), the 30 m/s vertical velocity isosurface is shaded in red, rainwater surfaces are shaded as transparent shells, and perturbation surface temperature is shaded on baseplane.

Our experience is that deep moist convection provides one of the most challenging tests for nonhydrostatic solvers, in terms of solver robustness (stability) and accuracy due to the significant latent heating occurring near the grid scale. Figure 6 shows the results of supercell simulations using the MPAS model and a rectangular mesh model with the initial sounding from Weisman and Klemp (1982) and unidirectional-shear hodograph. Mirror-image right and left moving supercells are produced in these simulations, and the right mover is shown in the figure. The two models produce very similar solutions, and we generally find that MPAS produces convective solutions of similar accuracy and quality as our state-of-the-art cloud models such as the Advanced Research WRF model (Skamarock and Klemp, 2008). We also find that MPAS is as robust and as efficient as the rectangular mesh models (e.g. ARW).

5 Summary

We have described the formulation of a fully compressible nonhydrostatic model discretized on (spherical) centroidal Voronoi meshes using a C-grid staggering of the prognostic variables. The Voronoi meshes are unstructured meshes that permit variable horizontal resolution, and our nonhydrostatic model solves the equations of motion directly on these unstructured meshes. The potential benefits of this formulation for the compressible flow solver are made possible by three advances. First, we are making use of the C-grid discretization techniques for Voronoi (hexagonal) meshes described by Thuburn et al. (2009) and Ringler et al. (2010) that solve the problems associated with the non-stationary geostrophic mode analyzed by Ničković et al (2002). Second, we are using higher-order transport operators as described in Skamarock and Gassman (2011); the higher-order transport scheme allows the MPAS model to produce solutions of similar accuracy to present day state-of-the-art cloud and mesoscale models, and also improves the large-scale response in early test simulations of baroclinic waves. Finally, MPAS is demonstrating computational efficiency similar to our rectangular mesh formulations on existing cache-based supercomputer architectures.

We have tested the MPAS nopnhydrostatic solver on large-scale flows (the Jablonowski and Williamson (2006) baroclinic wave on the sphere) and on small scale flows (e.g. supercell thunderstorms). MPAS has produced results comparable to other state-of-the-art models in these test. We are in the process of incorporating a full atmospheric physics suite into MPAS and we anticipate beginning to produce global NWP test forecasts early next year, along with full-physics variable-resolution tests in anticipation of using local refinement for NWP forecasts and for regional climate applications.

References

Arakawa, A. and V. Lamb, 1981: A potential enstrophy and energy conserving scheme for the shallow water equations. *Mon. Wea. Rev*, **109**, 18–36.

Jablonowski, C. and D. L. Williamson, 2006: A baroclinic instability test case for atmospheric model dynamical cores. *Quart. J. Roy. Meteor. Soc.*, **132**, 2943–2975.

Klemp, J. B., 2011: A terrain following coordinate with smoothed coordinate surfaces. *Mon. Wea. Rev.*, to be submitted.

Klemp, J. B., W. C. Skamarock, and J. Dudhia, 2007: Conservative split-explicit time integration methods for the compressible nonhydrostatic equations. *Mon. Wea. Rev.*, **135**, 2897–2913.

Klemp, J. B., W. C. Skamarock, and O. Furher, 2003: Numerical consistency of metric terms in terrain-following coordinates. *Mon. Wea. Rev.*, **131**, 1229–1239.

MacDonald, A. E., J. Middlecoff, H. T, and J.-L. Lee, 2010: A general method for modeling on irregular grids. *International Journal of High Performance Computing Applications*, in press.

Ničković, S., M. B. Gavrilov, and I. A. Tošić, 2002: Geostrophic adjustment on hexagonal grids. *Mon. Wea. Rev.*, **130**, 668–683.

Randall, D. A., 1994: Geostrophic adjustment and the finite-difference shallow-water equations. *Mon. Wea. Rev.*, **122**, 1371–1377.

Ringler, T., L. Ju, and M. Gunzburger, 2008: A multiresolution method for climate system modeling: application of spherical centroidal voronoi tessellations. *Ocean Dyn.*, **58**, 475–498.

Ringler, T., J. Thuburn, J. B. Klemp, and W. C. Skamarock, 2010: A unified approach to energy conservation and potential vorticity dynamics for arbitrarily-structured C-grids. *J. Comp. Phys.*, **229**, 3065–3090.

Sadourny, R., 1975: The dynamics of nite-difference models of the shallow-water equations. *J. Atmos. Sci.*, **32**, 680–698.

Sadourny, R. and C. Basdevant, 1985: Parameterization of subgrid scale barotropic and baroclinic eddies in quasi-geostrophic models - anticipated potential vorticity method. *J. Atmos. Sci..*, **42**, 1353–1363.

Skamarock, W. C. and A. Gassman, 2011: Conservative transport schemes for spherical geodesic grids: High-order flux operators for ODE-based time integration. *Mon. Wea. Rev.*, to be submitted.

Skamarock, W. C. and J. B. Klemp, 2008: A time-split nonhydrostatic atmospheric model for weather research and forecasting applications. *J. Comp. Phys.*, **227**, 3465–3485.

Thuburn, J., 2008: Numerical wave propagation on the hexagonal C-grid. *J. Comp. Phys.*, **227**, 5836–5858.

Thuburn, J., T. Ringler, W. C. Skamarock, and J. B. Klemp, 2009: A unified approach to energy conservation and potential vorticity dynamics for arbitrarily-structured C-grids. *J. Comp. Phys.*, **228**, 8321–8335.

Weisman, M. L. and J. B. Klemp, 1982: The dependence of numerically simulated convective storms on vertical wind shear and buoyancy. *Mon. Wea. Rev.*, **110**, 504–520.

Wicker, L. J. and W. C. Skamarock, 2002: Time-splitting methods for elastic models using forward time schemes. *Mon. Wea. Rev.*, **130**, 2088–2097.